JACS
JOURNAL OF THE AMERICAN CHEMICAL SOCIETY

Communication

pubs.acs.org/JACS

Galvanic Replacement Coupled to Seeded Growth as a Route for Shape-Controlled Synthesis of Plasmonic Nanorattles

Lakshminarayana Polavarapu,[*,†,‡,⊗,#] Daniele Zanaga,[§,⊗] Thomas Altantzis,[§] Sergio Rodal-Cedeira,[‡] Isabel Pastoriza-Santos,[‡] Jorge Pérez-Juste,[‡] Sara Bals,[*,§] and Luis M. Liz-Marzán[*,†,∥,⊥]

[†]Bionanoplasmonics Laboratory, CIC biomaGUNE, Paseo de Miramón 182, 20009 Donostia-San Sebastian, Spain

[‡]Departamento de Química Física, Universidade de Vigo, 36310 Vigo, Spain

[§]EMAT, University of Antwerp, Groenenborgerlaan 171, B-2020 Antwerp, Belgium

[∥]Ikerbasque, Basque Foundation for Science, 48013 Bilbao, Spain

[⊥]CIBER de Bioingeniería, Biomateriales y Nanomedicina, CIBER-BBN, 20009 Donostia-San Sebastián, Spain

Supporting Information

ABSTRACT: Shape-controlled synthesis of metal nanoparticles (NPs) requires mechanistic understanding toward the development of modern nanoscience and nanotechnology. We demonstrate here an unconventional shape transformation of Au@Ag core−shell NPs (nanorods and nanocubes) into octahedral nanorattles via room-temperature galvanic replacement coupled with seeded growth. The corresponding morphological and chemical transformations were investigated in three dimensions, using state-of-the-art X-ray energy-dispersive spectroscopy (XEDS) tomography. The addition of a reducing agent (ascorbic acid) plays a key role in this unconventional mechanistic path, in which galvanic replacement is found to dominate initially when the shell is made of Ag, while seeded growth suppresses transmetalation when a composition of Au:Ag (∼60:40) is reached in the shell, as revealed by quantitative XEDS tomography. This work not only opens new avenues toward the shape control of hollow NPs beyond the morphology of sacrificial templates, but also expands our understanding of chemical transformations in nanoscale galvanic replacement reactions. The XEDS electron tomography study presented here can be generally applied to investigate a wide range of nanoscale morphological and chemical transformations.

Nanoscale galvanic replacement is a versatile and elegant approach that has been widely employed to transform solid metal nanoparticles (NPs) into multimetallic hollow NPs with complex architectures, in which pore size and chemical composition determine the optical and catalytic properties.[1−8] Similar transformations can be carried out on Au@Ag core−shell NPs, thereby leading to the formation of plasmonic nanorattles, which have been reported to exhibit improved plasmonic activity (e.g., for surface-enhanced Raman scattering (SERS)), refractive index sensitivity, and catalytic activity as compared to their solid counterparts.[9,10] Internal electromagnetic hotspots in plasmonic nanorattles render them unique properties for plasmon-enhanced applications such as SERS, drug delivery, and photothermal therapies.[9,11,12] It has been widely observed that hollow NPs or plasmonic nanorattles obtained via galvanic replacement reactions preserve the morphology of the sacrificial templates, while excess transmetalation leads to fragmentation of such hollow particles.[1,3,4,9,11,13,14] We recently demonstrated the unconventional transformation of cubic Ag NPs into octahedral nanocages with complex metal distribution, when the reaction was carried out in a chlorinated organic solvent, indicating a high sensitivity to the reaction conditions.[2] Such unconventional morphological transformations have not been described for plasmonic nanorattles.[9] Here we demonstrate the shape control of plasmonic nanorattles beyond their template morphology through the transformation of Au@Ag core−shell nanorods (NRs) and nanocubes (NCs) into octahedral nanorattles via galvanic replacement with $HAuCl_4$ at room temperature, but in the presence of a mild reducing agent. In this case, no fragmentation was observed but rather seeded growth into a different morphology.[13] Although the mechanism of galvanic replacement reaction on Ag NPs has been well studied, mainly through morphological changes,[1,3,4,8,13,15] the mechanism involved in the transmetalation of core−shell NPs and their final chemical architectures is still poorly understood.[9,10] A thorough mechanistic analysis of galvanic replacement is possible by means of advanced electron tomography techniques, which enable simultaneous visualization of both morphological and chemical architectures of NPs in three dimensions (3D) at each step.[2,16] We demonstrated in recent works the uniqueness of qualitative and quantitative X-ray energy-dispersive spectroscopy (XEDS) tomography to understand complex hetero-nanostructures.[17,18] Quantitative XEDS tomography revealed that galvanic replacement dominates in the presence of a pure Ag shell, while at a Au:Ag composition of ∼60:40 transmetalation is suppressed, and seeded growth is favored when a larger amount of $HAuCl_4$ is added. Single-crystalline Au NRs (Figure S1) were used as seeds for the preparation of monodisperse Au@Ag core−shell NRs by epitaxial growth (see Supporting Information for details on the synthesis). Au@Ag NRs were then reacted with $HAuCl_4$ in the presence of ascorbic acid (AA).[3] The progress of the reaction was monitored by characterization of the products (obtained with different amounts of $HAuCl_4$), using UV−visible−NIR spectroscopy and transmission electron microscopy (TEM). XEDS

Received: June 29, 2016
Published: August 24, 2016

ACS Publications © 2016 American Chemical Society

DOI: 10.1021/jacs.6b06706
J. Am. Chem. Soc. 2016, 138, 11453−11456

tomography experiments were performed on selected samples toward a deeper mechanistic analysis. Significant differences with respect to conventional nanoscale galvanic replacement (between Ag NPs and $HAuCl_4$) were observed when excess $HAuCl_4$ was used. Whereas the solution would typically become red due to the breakdown of the shell structure and formation of Au spheroids,[1,2,11,13] in the presence of AA the colloid turned blue, with no sign of NP degradation. The UV−visible−NIR extinction spectra of Au@Ag core−shell NRs before and after titration with different amounts of $HAuCl_4$ are shown in Figure 1.

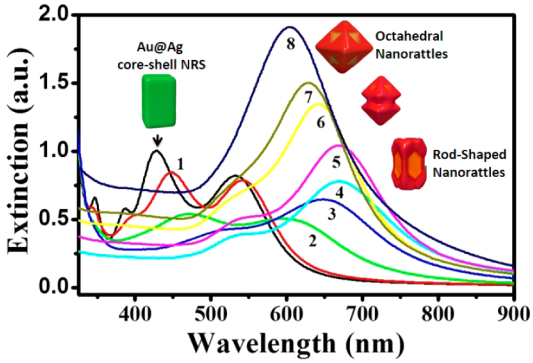

Figure 1. UV−visible−NIR extinction spectra of Au@Ag core−shell nanorods before (1) and after (2−8) galvanic replacement with increasing amounts of $HAuCl_4$. Insets: Selected 3D schematic models, drawn based on electron tomography.

Core−shell NRs display a longitudinal localized surface plasmon resonance (LSPR) at 533 nm and a transverse dipolar LSPR mode at 428 nm, as well as two higher order plasmon modes.[19] As the galvanic replacement reaction proceeds, the low-energy modes vanish while the longitudinal and transverse LSPR bands red-shift and dampen as the amount of $HAuCl_4$ is increased. However, upon further increasing the amount of $HAuCl_4$ (samples 5−8), the bands blue-shift back with increasing peak intensities. These spectral changes significantly differ from those in standard nanoscale galvanic replacement on Ag NPs, in the absence of AA (Figure S2).[2,13] A conventional nanoscale galvanic replacement reaction is exemplified in Figure S2, showing that the addition of higher amounts of $HAuCl_4$ leads to breakdown of nanocages due to excess transmetalation, resulting in the disappearance of the nanoshell plasmon peak.

In order to investigate the unconventional growth process of octahedral nanorattles, complementary analyses were carried out via morphological NP characterization at different degrees of reduction, by means of TEM, high-angle annular dark-field scanning transmission electron microscopy (HAADF-STEM), and XEDS mapping (Figure 2; see Figure S3 for an overview of larger area TEM images). Although obvious morphological changes are observed in the TEM and HAADF-STEM images, it is however unclear how the reaction initiates on the core−shell NPs (Figure 2b). After initiation of the galvanic reaction with a small amount of $HAuCl_4$ (0.05 mL, 0.5 mM) (Figure 2b), the surface of the particles appears irregular due to the initial oxidation of Ag atoms. Upon further addition of $HAuCl_4$, Au is deposited on the outer Ag surface, while voids start to be observed, as expected in galvanic replacement. When more $HAuCl_4$ is added (Figure 2d−f), further deposition of Au on the external NP surface is clearly shown by the XEDS maps, resulting in what appear to be hollow octahedrons containing the initial gold rods. This is thus an example of unconventional morphological changes, somehow similar to those previously reported for Ag NCs in organic solvent.[2] However, 2D TEM/XEDS characterization does not provide sufficient information on either the morphological or chemical architectures of the intermediate and final nanocrystals. It is particularly surprising to see overgrowth instead of NP fragmentation due to transmetalation of the Au/Ag alloy with addition of higher amounts of $HAuCl_4$, which has not been observed in previous studies.

Unambiguous determination of the mechanism behind these nanoscale transformations can be achieved by carrying out electron tomography combined with XEDS in 3D. Tilt series of HAADF-STEM images and XEDS maps (Figure S4) were acquired and combined in a synergistic manner by the use of a recently developed approach.[18] The results of the analysis are summarized in Figure 3 (see Movies S1−S5 for 3D visualizations of particles in stages i−v; the 3D reconstruction images in Figure 3, panels i−v, correspond to the 2D images of Figure 2b−f, respectively). From the 3D reconstructions it appears that, in the first stages (Figure 3a,b-i and Movie S1) the Ag shell is eroded

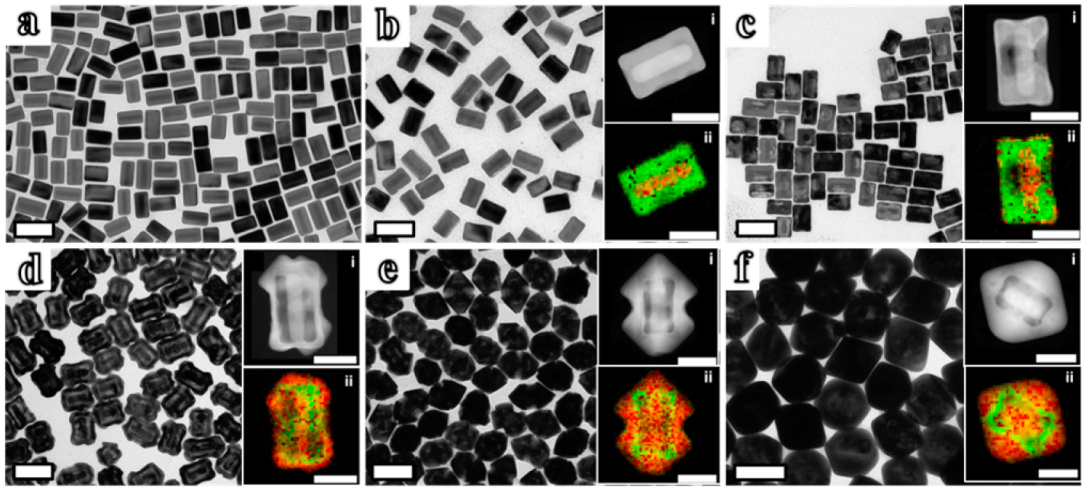

Figure 2. TEM images of Au@Ag core−shell NRs before (a) and after (b−f) galvanic replacement with increasing amounts of 0.5 mM $HAuCl_4$. The corresponding HAADF-STEM images (i) and XEDS maps (ii) (green, Ag; red, Au) are included as insets in panels b−f. Scale bars for the TEM images and the insets are 100 and 40 nm, respectively.

DOI: 10.1021/jacs.6b06706
J. Am. Chem. Soc. 2016, 138, 11453−11456

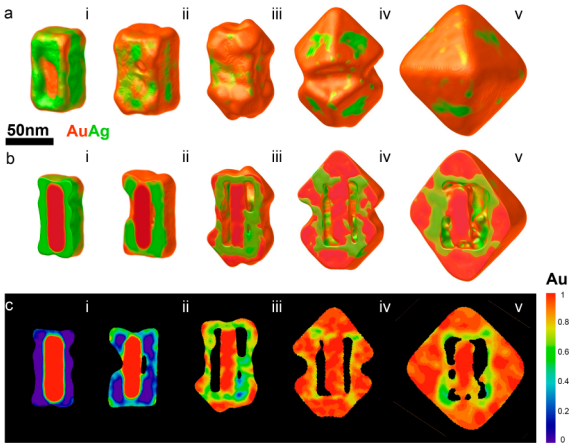

Figure 3. Quantitative XEDS tomography imaging. Transformation of Au@Ag NRs into octahedral nanorattles with addition of increasing amounts of $HAuCl_4$ in consecutive reactions (stages i-v). (a) 3D reconstructions showing Au (orange) and Ag (green) at each transformation. (b) Inner view of the 3D reconstructions. (c) XEDS 3D quantified reconstruction slices, where the color scale on the right reflects the percentage of Au.

due to the start of the galvanic replacement reaction, with formation of grooves on the Ag surface and deposition of small amounts of Au on the edges and corners of the rectangular cuboid. The higher density of Au on the corners as compared to the edges provides experimental evidence for higher reactivity of sharper sites, which agrees with previous reports on the difference in reactivity of truncated and sharp Ag NCs reported by Lu et al.[13] and the seed-mediated palladium deposition on edges of Au NCs reported by DeSantis et al.[20] High-resolution STEM images further confirm the epitaxial relation between Au and Ag at the corners (Figure S5). As the reaction proceeds (Figure 3a,b-ii and Movie S2), a thin layer of Au is deposited on the surface of the cuboid with holes on the facets (Figure S4). To our knowledge, these results provide the first experimental evidence for the reactivity of corners > edges > facets of a cuboid. Even though it is extremely difficult to identify the deposition of a thin Au shell either on edges or on facets based on 2D EDX mapping alone, 3D XEDS tomography revealed accurate visualization of the chemical architecture of the particles. Interestingly, tomography data shows that pitting takes place on more than one facet of the Au@Ag core−shell NRs, through which the oxidized Ag^+ ions leach out (Figure S4), which is different compared to the case of Ag NCs in which this occurs on one of the six facets only. With increasing the amount of $HAuCl_4$, the hollow area extends with formation of an Au/Ag shell surrounded by a solid layer of Au, where {111} facets start to grow (Figure 3a,b-iii, Movie S3, and Figure S4). Excess addition of $HAuCl_4$ leads to the further growth of {111} facets (Figure 3a,b-iv and Movie S4) which eventually complete the formation of octahedral nanorattles, encasing an Au rod and showing a complex chemical distribution (Figure 3a,b-v and Movie S5). High-resolution STEM images (Figure S5) show that these nanorattles retain a monocrystalline structure. A more detailed analysis of the chemical transformations at each stage can be obtained by quantitative 3D XEDS reconstruction (Figure 3c),[18] which yields percentages of Au and Ag, in each analyzed particle (see further details in Figure S6 and Tables S1 and S2). As expected, we see a decrease of Ag and an increase of Au concentrations with increasing addition of $HAuCl_4$ (stages i−iii, Table S1). At stage iii, formation of a hollow Au/Ag alloy shell, with a composition of 60:40, can be clearly distinguished (Figure 3c-iii). Further addition of $HAuCl_4$ decreases the overall silver content as a consequence of Au overgrowth. Interestingly, XEDS tomography revealed that the inner Au/Ag alloy shell formed in stage iii retains the 60:40 Au/Ag composition (Figure 3c-v). As discussed above, transmetalation of Au/Ag alloy nanocages generally leads to fragmentation (Figure S2).[13] However, in the present system, seeded growth takes place on the outer Au/Ag shell, which is likely related to $HAuCl_4$ reduction by AA, in a manner similar to the widely used seeded growth of Au NPs.[21,22] EDX mapping of octahedral nanorattles shows silver residues in the outer shell. These were initially ascribed to the co-reduction of Ag ions together with Au ions in the presence of AA, similar to the so-called seed-mediated co-reduction as reported by Skrabalak and co-workers.[23] However, 3D XEDS tomography suggests that there is no Ag in the outer shell, suggesting the residual signals arise from background noise of 2D EDX mappings that could lead to misinterpretation of the results. Thus, 3D XEDS tomography unambiguously revealed the chemical architecture of the resulting nanorattles.

Interestingly, we note that this unusual transformation of the morphology and chemical architecture can also be observed when starting with NPs with different morphology, such as Au@Ag core−shell NCs (Au nanooctahedra@Ag nanocubes, NO@NC), indicating the versatility of this approach (Figure 4 and

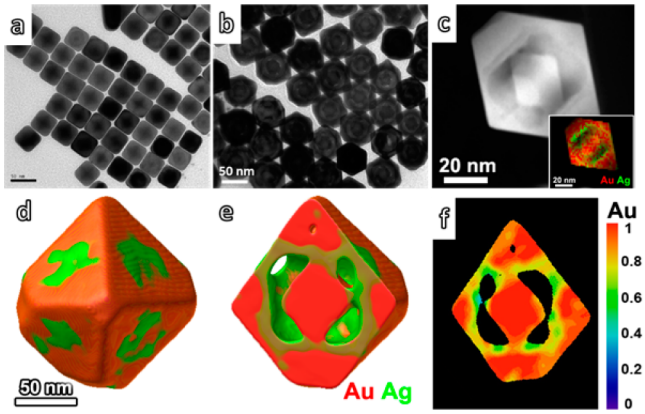

Figure 4. (a) TEM image of Au nanooctahedra@Ag nanocubes. (b−f) TEM (b), HAADF-STEM (inset: 2D XEDS mapping) (c), view of quantitative XEDS 3D reconstruction showing Au (orange) and Ag (green) (d), a slice through the reconstruction (e), and XEDS 3D quantified reconstruction slice (f) of octahedral nanorattles with Au octahedral as core, obtained via galvanic replacement between Au NO @ Ag NCs and $HAuCl_4$.

Figure S7). In a conventional nanoscale galvanic replacement reaction on Au@Ag core−shell NCs, we would expect to obtain cubic nanorattles. In this case, however, we find again that the resulting structures display an octahedral shape (Figure 4; see Figure S7 for large-area TEM and SEM images). Analysis by HAADF-STEM tomography and 3D-XEDS revealed that the final product is analogous in its complex chemical structure to the samples obtained when starting from Au@Ag NRs, with the only difference being the octahedral cores in the center (Figure 4 and Movie S6).[18] This also includes the composition of the Au/Ag alloy inner shell (60:40; see Figure 4f). These observations generalize our conclusions regarding the effect of AA on the galvanic replacement reaction on Ag@Au core−shell NPs. Two important effects arise from the presence of AA, which should be

DOI: 10.1021/jacs.6b06706
J. Am. Chem. Soc. 2016, 138, 11453−11456

considered: (i) the reduction of Au^{3+} into Au^{+} by AA significantly decreases the rate of galvanic replacement because only one Ag atom is involved, rather than three (in the absence of AA),[24,25] which allows better control over the reaction progress; and (ii) the mild reducing nature of AA can also lead to the catalytic reduction of Au^{+} into Au^{0} on the metal NPs surface (seeded growth).[23] The present quantitative tomography study suggests that galvanic replacement on Ag shells dominates during the early stages, whereas Au overgrowth on the outer Au/Ag shell hinders transmetalation on the alloy, in the presence of AA.[26,27] We hypothesize that the reduction of Au^{3+} to Au^{+} by AA plays an essential role by changing the kinetics and stoichiometry of the galvanic replacement reaction. This may also influence the different chemical architecture of the resulting octahedral nanorattles, which is radically different to what has been previously reported for galvanic replacement in Ag NCs, both at room temperature and at 100 °C.[2,3,13] No Kirkendall growth is observed here, unlike the case of galvanic replacement on Ag NCs, where it leads to double-walled nanoboxes.[3]

In summary, we have demonstrated an unconventional morphological transformation of Au@Ag core−shell NPs (either NRs or NCs) into octahedral nanorattles via galvanic replacement reaction coupled with co-reduction by AA. State-of-the-art X-ray energy-dispersive spectroscopy (XEDS) tomography revealed that galvanic replacement dominates in the case of a pure Ag shell, while seeded growth suppresses transmetalation of Au/Ag (~60:40) shell at later stages, eventually leading to an octahedral morphology with complex elemental distribution. This study suggests that the shape of the hollow nanoparticles can be controlled beyond their template morphology in the presence of reducing agents, thus enabling additional tunability of their optical properties. In addition, it advances our understanding of nanoscale galvanic replacement reaction in the presence of reducing agents, which can lead to unconventional shape transformations. Owing to its high versatility, 3D XEDS tomography can be applied to understanding the growth mechanisms in a wide range of nanoscale shape and chemical transformations.

■ ASSOCIATED CONTENT

Supporting Information

The Supporting Information is available free of charge on the ACS Publications website at DOI: 10.1021/jacs.6b06706.

Experimental details, spectra and TEM images, and information about the 3D XEDS reconstructions, including Figures S1−S7 and Tables S1 and S2 (PDF)
Movie S1, animated view of the quantitative 3D XEDS tomographic reconstructions of samples obtained via galvanic replacement between Au@Ag core−shell NRs and increasing amounts of $HAuCl_4$, stage i (MPG)
Movie S2, 3D XEDS reconstruction, stage ii (MPG)
Movie S3, 3D XEDS reconstruction, stage iii (MPG)
Movie S4, 3D XEDS reconstruction, stage iv (MPG)
Movie S5, 3D XEDS reconstruction, stage v (MPG)
Movie S6, animated view of the quantitative 3D XEDS tomographic reconstruction of octahedral nanorattles obtained via galvanic replacement between Au@Ag core−shell nanocubes (NO@NC) and $HAuCl_4$ (MPG)

■ AUTHOR INFORMATION

Corresponding Authors

*lakshmi@uvigo.es
*sara.bals@uantwerpen.be
*llizmarzan@cicbiomagune.es

Present Address

#L.P.: Department of Physics, Ludwig-Maximilians-Universität München, Munich, Germany

Author Contributions

⊗L.P. and D.Z. contributed equally to this work.

Notes

The authors declare no competing financial interest.

■ ACKNOWLEDGMENTS

This work has been funded by the European Research Council (ERC Advanced Grant No. 267867-PLASMAQUO, ERC Starting Grant No. 335078-COLOURATOMS) and Spanish MINECO (Grants MAT2013-45168-R, MAT2013-46101-R).

■ REFERENCES

(1) Skrabalak, S. E.; Chen, J. Y.; Sun, Y. G.; Lu, X. M.; Au, L.; Cobley, C. M.; Xia, Y. N. *Acc. Chem. Res.* **2008**, *41*, 1587.
(2) Goris, B.; Polavarapu, L.; Bals, S.; Van Tendeloo, G.; Liz-Marzán, L. M. *Nano Lett.* **2014**, *14*, 3220.
(3) Gonzalez, E.; Arbiol, J.; Puntes, V. F. *Science* **2011**, *334*, 1377.
(4) Oh, M. H.; Yu, T.; Yu, S. H.; Lim, B.; Ko, K. T.; Willinger, M. G.; Seo, D. H.; Kim, B. H.; Cho, M. G.; Park, J. H.; Kang, K.; Sung, Y. E.; Pinna, N.; Hyeon, T. *Science* **2013**, *340*, 964.
(5) Tao, A. R.; Habas, S.; Yang, P. D. *Small* **2008**, *4*, 310.
(6) Slater, T. J. A.; Macedo, A.; Schroeder, S. L. M.; Burke, M. G.; O'Brien, P.; Camargo, P. H. C.; Haigh, S. J. *Nano Lett.* **2014**, *14*, 1921.
(7) Chen, J. Y.; Wiley, B.; Li, Z. Y.; Campbell, D.; Saeki, F.; Cang, H.; Au, L.; Lee, J.; Li, X. D.; Xia, Y. N. *Adv. Mater.* **2005**, *17*, 2255.
(8) Hong, X.; Wang, D. S.; Cai, S. F.; Rong, H. P.; Li, Y. D. *J. Am. Chem. Soc.* **2012**, *134*, 18165.
(9) Liu, K.-K.; Tadepalli, S.; Tian, L.; Singamaneni, S. *Chem. Mater.* **2015**, *27*, 5261.
(10) Khalavka, Y.; Becker, J.; Sönnichsen, C. *J. Am. Chem. Soc.* **2009**, *131*, 1871.
(11) Xiong, W.; Mazid, R.; Yap, L. W.; Li, X.; Cheng, W. *Nanoscale* **2014**, *6*, 14388.
(12) Lohse, S. E.; Murphy, C. J. *J. Am. Chem. Soc.* **2012**, *134*, 15607.
(13) Lu, X. M.; Tuan, H. Y.; Chen, J. Y.; Li, Z. Y.; Korgel, B. A.; Xia, Y. N. *J. Am. Chem. Soc.* **2007**, *129*, 1733.
(14) Sun, Y. G.; Xia, Y. N. *Science* **2002**, *298*, 2176.
(15) Wang, W. S.; Dahl, M.; Yin, Y. D. *Chem. Mater.* **2013**, *25*, 1179.
(16) Midgley, P. A.; Dunin-Borkowski, R. E. *Nat. Mater.* **2009**, *8*, 271.
(17) Pfannmöller, M.; Heidari, H.; Nanson, L.; Lozman, O. R.; Chrapa, M.; Offermans, T.; Nisato, G.; Bals, S. *Nano Lett.* **2015**, *15*, 6634.
(18) Zanaga, D.; Altantzis, T.; Polavarapu, L.; Liz-Marzan, L. M.; Freitag, B.; Bals, S. *Part. Part. Syst. Charact.* **2016**, *33*, 396.
(19) Jiang, R.; Chen, H.; Shao, L.; Li, Q.; Wang, J. *Adv. Mater.* **2012**, *24*, OP200.
(20) DeSantis, C. J.; Sue, A. C.; Bower, M. M.; Skrabalak, S. E. *ACS Nano* **2012**, *6*, 2617.
(21) Weiner, R. G.; Kunz, M. R.; Skrabalak, S. E. *Acc. Chem. Res.* **2015**, *48*, 2688.
(22) Tsao, Y.-C.; Rej, S.; Chiu, C.-Y.; Huang, M. H. *J. Am. Chem. Soc.* **2014**, *136*, 396.
(23) Weiner, R. G.; Skrabalak, S. E. *Chem. Mater.* **2016**, *28*, 4139.
(24) Au, L.; Chen, Y.; Zhou, F.; Camargo, P. H. C.; Lim, B.; Li, Z.-Y.; Ginger, D. S.; Xia, Y. *Nano Res.* **2008**, *1*, 441.
(25) Au, L.; Lu, X.; Xia, Y. *Adv. Mater.* **2008**, *20*, 2517.
(26) Yang, Y.; Liu, J.; Fu, Z.-W.; Qin, D. *J. Am. Chem. Soc.* **2014**, *136*, 8153.
(27) Zhang, J.; Winget, S. A.; Wu, Y.; Su, D.; Sun, X.; Xie, Z.-X.; Qin, D. *ACS Nano* **2016**, *10*, 2607.

DOI: 10.1021/jacs.6b06706
J. Am. Chem. Soc. 2016, 138, 11453−11456